European Journal of Physics

Undergraduate quantum optics – Experimental steps to quantum physics

Undergraduate Quantum Optics – Experimental Steps to Quantum Physics

Ruediger Scholz[1], Gunnar Friege[2], Kim-Alessandro Weber[2]

[1]Institut fuer Quantenoptik, Leibniz Universitaet Hannover

[2]Institut fuer Didaktik der Mathematik und Physik, Leibniz Universitaet Hannover

Abstract

We report on a step-by-step-series of experiments from statistical optics with classical light to undergraduate quantum optics (UQO) with single photon states, particularly suitable to pave an introductory way to quantum phenomena. We built up a progressive process analysing temporal variations of the irradiance of light discerned by measuring the value of the non delayed second order correlation function $g^{(2)}(\tau = 0)$. We demonstrate how Poisson distributed photoelectron counts from constant irradiance ($g^{(2)}(0) = 1$) can be used to calibrate the apparatus. Measurements with harmonically modulated irradiance of Poissonian light gives an introduction into $g^{(2)}(0)$-correlation-analysis. After these introductory steps we demonstrate photon bunching with (pseudo-) thermal light ($g^{(2)}(0) \approx 2$), and finally show quantum antibunching of photons in Fock states ($g^{(2)}(0) \approx 0$). All measurements are in excellent agreement with the theoretical predictions.

1 Introduction

Since 40 years photoelectron counting statistics has proven to be a powerful tool to investigate characteristics of light (Saleh, 1978). We have experienced that statistical optical experiments are well suited to construct an experimental based "pedestrian approach" to quantum physics by focussing on light fluctuations. In this sense optical correlation experiments in undergraduate laboratories may contribute to a comprehensive, modern physics education figuring out the differences between classical and quantum light. These experiments help to enter the realm of photon counting and quantum optics and may lead to a resilient physical intuition (Thorn et. al., 2004, Galvez & Beck, 2017). This paper describes a series of such experiments, set up to accompany a coherent optics lesson after the second year of studying. We would like to appreciate the work published by Brett Pearson and David Jackson in (Pearson & Jackson, 2010). Much of their arguments guided this work.

Section 2 presents the basic photoelectron counting technique. The experiments rely on coincidence measurements with a small coincidence window width ($w = 5$ ns). This technique allows to study light fluctuations evaluating the non delayed second-order correlation function $g^{(2)}(\tau = 0)$. For the logic circuit of the counting unit we expanded the function range of the field programmable gate array (FPGA) design published by other groups (e. g. a phase-locked-loop for synchronized pulse shortening; see appendix C); here we would like to emphasize the quite pioneering counting scheme of Branning et. al. (Branning, Bhandari, and Beck, 2009).

In section 3 we present details and results of the experiments. Recently we demonstrated a low cost LED-set-up to produce (pseudo-) thermal light with a perfect geometrical distribution of photoelectron counts (Scholz, Friege, & Weber, 2016). Now, in the next step, we expand the ideas to statistical optics with harmonically modulated irradiance (Fox, 2006) and finally with single-photon Fock light. As a source for correlated photons we use spontaneous parametric down conversion (PDC), increasingly common in undergraduate laboratories.

Student's guide (https://www.idmp.uni-hannover.de/256.html) To ensure an appropriate scope of this article, we decided to swap out some of the content. Original data from single-photon-experiments (for classroom bound evaluation), details to align the setup and to build a copy of our counting unit are available from our website.

2 Fluctuation analysis

2.1 The binary detection scheme

Introductory quantum optics textbooks present the analysis of field fluctuations as a basic concept to analyse light fields within the boundaries of classical Maxwell physics and in the quantum regime as well. Let us start with some basics of "light counting" (for a systematic presentation of the theory see Loudon, 2000).

Field correlation: Classical optical fields are well described by the irradiance derived from electromagnetic waves. The somehow vague term *intensity* and the radiometric term *irradiance* (i.e. the radiation power reaching an area A of the detector divided by the area A, in W/m^2) are often used synonymously. Here we prefer the term irradiance. Further it should be stated that $I(t)$ represents the cycle-averaged irradiance, thus we may dispense with a particular marking of this standard averaging process. For quasi-monochromatic waves with a slowly varying amplitude $E_0(t)$ we get $E(z,t) = E_0(t)\sin(\omega t - kz) \Rightarrow I(t) = \varepsilon_0 c \left\langle E^2(t) \right\rangle_t \approx \frac{1}{2}\varepsilon_0 c E_0{}^2(t)$.

For classical waves the slowly varying amplitude $E_0(t)$ is connected to the frequency spectrum via the usual Fourier transformation

$$E(\Omega) = \frac{1}{2\pi}\int_{-\infty}^{\infty} \mathrm{d}t E(t) \exp \mathrm{i}\Omega t \,.$$

The line shape $I(\Omega)$ is then derived from an auto-correlation of the field strength:

$$\begin{aligned} I(\Omega) = \left|E(\Omega)\right|^2 &= \frac{1}{4\pi^2}\int_{-\infty}^{\infty} \mathrm{d}t' \int_{-\infty}^{\infty} \mathrm{d}t E(t') E^*(t) \exp\left(i\Omega(t'-t)\right) \\ &= \frac{1}{4\pi^2}\int_{-\infty}^{\infty} \mathrm{d}\tau \underbrace{\int_{-\infty}^{\infty} \mathrm{d}t E(t+\tau) E^*(t)}_{\to \frac{1}{T}\int_0^T \mathrm{d}t E(t+\tau)E^*(t) = \left\langle E^*(t)\cdot E(t+\tau)\right\rangle_T} \exp(i\Omega\tau) \end{aligned}$$

For a sampling time T large compared to the delay τ and for an angular frequency at the center of the line we get the auto-correlation of the light field $\langle E^*(t) \cdot E(t + \tau)\rangle$, analyzing typical coherence features from first order interference phenomena. The essential work from Hanbury Brown and Twiss (Hanbury Brown, Twiss, 1956) tells us that the analysis of light field fluctuations is based on irradiance correlation (eq. (2.3)).

Sample averaging: The sampling characteristic of the detectors requires a further averaging over the sampling period T. In this case the irradiance measured by the detector at time t is given by the average value $\left\langle I(t)\right\rangle_T$:

$$\left\langle I(t)\right\rangle_T = \frac{1}{T}\int_t^{t+T} \mathrm{d}t' I(t') \,. \tag{2.1}$$

As our detectors are running in a binary Geiger mode they convert the continuous input irradiance into a pulse train. The counting rate $\langle N\rangle/T$ of the pulses is proportional to the input irradiance. From semi-classical detection theory we get the mean number of impulses $\langle N\rangle_T$ generated from a mean irradiance $\langle I(t)\rangle_T$ impinging on the detector during the sampling interval T (from the output channel 3 und 4 of the beam splitter, see fig. 1):

$$\left\langle N_3\right\rangle_T = \eta_3 T\left\langle I_3(t)\right\rangle_T \text{ and } \left\langle N_4\right\rangle_T = \eta_4 T\left\langle I_4(t)\right\rangle_T \,, \tag{2.2}$$

here η characterizes the detection efficiency of the detector not specified at this point (Loudon, 2000). For a more rigorous derivation of counting probabilities see appendix A.

2.2 Correlation measurement: Twofold coincidences

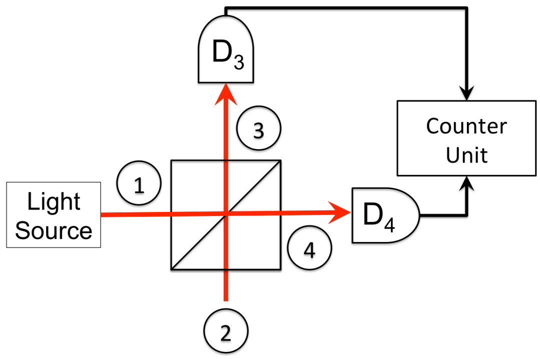

1 The double-detector arrangement of the Hanbury Brown-Twiss interferometer: Input at Channel 1 and 2, output at channel 3 and 4

A countless number of educational experimental settings rely on the irradiance-interferometer shown in fig. 1 first introduced by Hanbury Brown and Twiss to measure correlation effects in light beams (Hanbury Brown, Twiss, 1956). The light fields registered by two detectors D_3 and D_4 at the output channels of a 50:50 optical beam splitter are represented by the irradiance $I_3(t)$ resp. $I_4(t)$. The fluctuations of these light fields are analysed by studying the normalized correlation of the irradiance from the output channels of the beam splitter:

$$g^{(2)}_{3,4}(\tau) = \frac{\langle I_3(t) I_4(t+\tau)\rangle_T}{\langle I_3(t)\rangle_T \langle I_4(t+\tau)\rangle_T}$$

where τ specifies a possible delay between the detector signals $I_3(t)$ and $I_4(t+\tau)$. We emphasize that $g^{(2)}(\tau)$ is the irradiance analogue of the first-order correlation function $g^{(1)}(\tau)$ closely related to the contrast of interference fringes (Fox, 2006). For our purposes the analysis of coinciding pulses from D_3 and D_4 (fig. 1) is of special interest. Thus we will study light fluctuations from the correlation of non-delayed fields, $\tau = 0$, what will remarkably simplify the experiments, even for the observation of of single photon antibunching (for an excellent representation and overview see (Pearson & Jackson, 2010):

$$g^{(2)}_{3,4}(0) = \frac{\langle I_3(t) I_4(t)\rangle_T}{\langle I_3(t)\rangle_T \langle I_4(t)\rangle_T}. \tag{2.3}$$

For low irradiance using the binary detection scheme as described above, eq. (2.3) has to be converted into a discrete impulse version. Inserting eq. (2.2) the normalized correlation function eq. (2.3) can be rewritten

$$g^{(2)}_{3,4}(0) = \frac{\langle I_3(t) I_4(t)\rangle_T}{\langle I_3(t)\rangle_T \langle I_4(t)\rangle_T} = \frac{\langle N_3 \cdot N_4\rangle_T}{\langle N_3\rangle_T \langle N_4\rangle_T}. \tag{2.4}$$

In our experiments the correlation is determined from the measurement of the number of impulses coinciding within a small time window w:

- Coincidence counting involves at least two detectors sending pulses to a central counting unit (CCU).
- A two-fold coincidence is defined to be a sample of two pulses that are registered (nearly simultaneously) within a small time interval of width w. Using n detectors and an appropriate counting unit gives the opportunity to measure n-fold coincidence; our experiments are restricted to $n \leq 3$.

Coincidences may be accidental or caused by particular physics "hidden" in the fluctuations. For the accidental case $\langle N_3\rangle$ and $\langle N_4\rangle$ are independent, yielding $\langle N_3 \cdot N_4\rangle_T = \langle N_3\rangle_T \cdot \langle N_4\rangle_T$, regardless of T leading to $g^{(2)}_{34}(0) = 1$.

Let us now introduce the number $N_{34}(w)$ of 3-4-coincidences measured within the short time window w. It is reasonable that the rate of coincidences $N_{34}(w)/w$ is equal to the rate of correlated pulses during the sampling time T: $\langle N_3 \cdot N_4 \rangle / T$. In our experiments we measure $N_{34}(w)$. Rewriting eq. (2.4) gives the final equation:

$$g_{3,4}^{(2)}(0) = \frac{\langle N_3 \cdot N_4 \rangle_T}{\langle N_3 \rangle_T \langle N_4 \rangle_T} = \frac{N_{34}(w)}{\langle N_3 \rangle_T \langle N_4 \rangle_T} \frac{T}{w}. \tag{2.5}$$

2.3 Triple coincidences

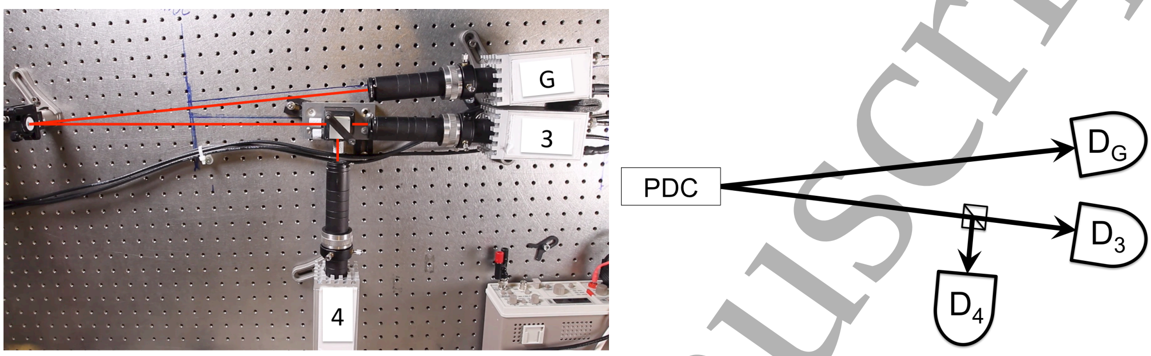

2 The gated single-photon-equipment

To produce correlated photons, we used the standard parametric-down-conversion (PDC) device. Fig. 2 shows the set up. The detectors D_3 and D_4 serve as signal detectors, while detector D_G delivers a trigger pulse (idler photon). In the experiments we are counting the number of impulses from D_3 and D_4 within a small time window w solely under condition that D_G had sent a trigger pulse. Let us write $N_{3|G}(w)$ and $N_{4|G}(w)$ for these conditioned single counting numbers and $N_{34|G}(w)$ for the conditioned coincidences during w. Then from eq. (2.5) we get for the correlation function

$$g_{3,4}^{(2)}(0) = \frac{N_{34|G}(w)}{\langle N_{3|G} \rangle_w \langle N_{4|G} \rangle_w} \frac{w}{w} = \frac{N_{34|G}(w)}{\langle N_{3|G} \rangle_w \langle N_{4|G} \rangle_w}. \tag{2.6}$$

Here we set $T = w$ because only pulses within the small time window w are counted. From elementary probability theory the connection between joint and conditioned probability is well known. The same holds for the corresponding count numbers: $N_{x|G} = N_{xG}/N_G$; inserting into eq. (2.6) we get:

$$g_{34G}^{(2)}(0) = \frac{N_{34G}(w)/N_G}{\langle N_{3G} \rangle_w \langle N_{4G} \rangle_w / N_G^2} = \frac{N_{34G}(w)}{\langle N_{3G} \rangle_w \langle N_{4G} \rangle_w} N_G. \tag{2.7}$$

N_{34G} is the number of triple coincidences for the three detectors, while N_{3G} and N_{4G} are the twofold coincidences between D_3 and D_G and D_4 and D_G respectively. N_{34G}, N_{3G} and N_{4G} are directly measured in the experiment.

2.4 Counting set up

Let us now describe the signal processing set up (for details of the complete apparatus see appendix C). The device has been built as a version of the coincidence counting unit (CCU) proposed in (Goodman, 1976 and Branning et. al., 2009) using AND-gates to detect coincident pulses. Core element of the CCU is a field programmable gate array (FPGA, fig. 3). In our CCU we used the programmable logic blocks of the FPGA to perform combinational logic functions and simple logic gates like AND and XOR. Due to the concentrated array structure it is possible to run the FPGA in a fast parallel processing mode of the input signals. A very precise controlling of the sampling time T could be realized by triggering the FPGA with a 50 MHz-real time clock.

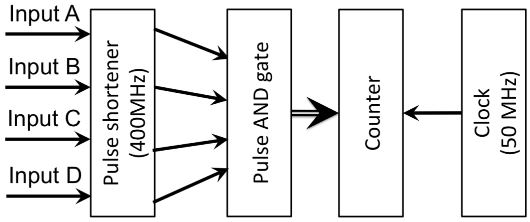

3 Block diagram of the FPGA unit; the circuit has been used to realize a pulse shortener, the AND gate and the 50 MHz real time clock

(1) Pulse-shaping: The 50 ns-detector pulse length from the avalanche diode (APD) is much to long for our purpose. We aimed at a coincidence window width $w \approx 5$ ns. Fig. 4 shows the pulse-shaping procedure. The process is accomplished by use of two copies of the incoming pulse of length T_P. One of them is delayed by τ' and logically inverted. Using these pulses as inputs of an AND gate, we obviously get the shaded high level output signal: The AND output will only be high for the time delay τ'. This temporal data-alignment of the two pulses has been achieved by a shift register with a 400 MHz-system-ticker (8-fold phase-locked-loop-signal from the 50-MHz-clock). Thus we could align a $\tau' \approx 2.5$ ns-delay between input and output of the shift register per 50-MHz-clock cycle. Technically the delay has been restricted to $n = 5$ clock cycles, leading to a proper pulse length $\tau = n \cdot \tau'$ (the real value of τ' has to be measured; see section 3.1).

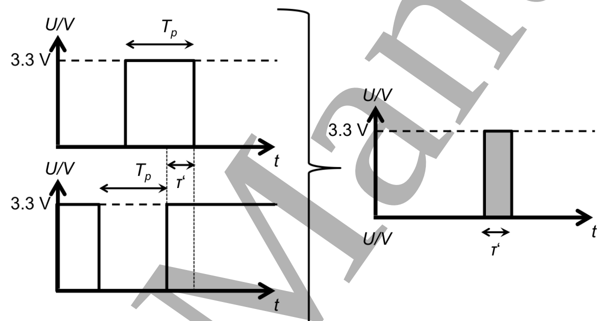

4 The pulse-shaping process

(2) Coincidence window: Two incoming and overlapping pulses of duration τ' will set the high level of an AND-gate from the leading edge of the first of the pulses until the trailing edge of the second one. From the overlapp of two 2.5 ns-pulses we thus get a coincidence window width $w \approx 2\tau' = 5$ ns. We measured the length of the coincidence window width in a quantum optics experimental setup, however with classical chaotic light from a LED. This light would solely produce accidental coincidences with $g_{3,4}^{(2)}(0) = 1$. Then from eq. (2.5) w can be evaluated (see section 3.1)

(3) Coincidence processing: From 15 single counters of our CCU, all running in a parallel mode, we used 3 counters for the input channels, 3 counters for two-fold coincidences and one for triple coincidences.

(4) Adjusting the sampling time T: To adjust a proper sampling time T the counter has been triggered by a 50 MHz signal: A sampling time $T = 1$ s could be realized by setting an open gate for $5{\cdot}10^7$ ticker cycles from the clock.

3 Experiments

Now we present the series of experiments culminating in an experiment demonstrating the Fock state antibunching phenomenon. A compilation of the complete program is shown in the following table. The presentation of the experiments in the particular subsections gives detailed explanations.

1	$g_{34}^{(2)}(0)$-Measurement with uncorrelated light	Calibration: Measurement of the window width w	Uncorrelated light yields $g_{34}^{(2)}(0)=1$ and we can deduce the temporal window width w
2	$g_{34G}^{(2)}(0)$-Measurement with uncorrelated light	Performance of the AND-gate electronics for triple coincidences	Pure accidental coincidences yields $g_{34G}^{(2)}(0)=1$ and we can normalize the measurement of triple coincidences to 1 for uncorrelated light
3	$g_{34}^{(2)}(0)$-Measurement Poissonian light	$I(t)=\langle I(t)\rangle_T = const.$	$g_{34}^{(2)}(0)=1$
4	$g_{34}^{(2)}(0)$-Measurement modulated irradiance	$\langle I(t)\rangle_T = I_0(1+\lvert S\rvert\sin\omega t)$ $\lvert S\rvert \le 1$	$g_{34}^{(2)}(0)=1+S^2/2$
5	$g_{34}^{(2)}(0)$-Measurement (Pseudo-) thermal light	$\langle I(t)\rangle_T = I_0+\Delta I_{\text{th}}$	$g_{34}^{(2)}(0)=2$
6	$g_{34}^{(2)}(0)$-Measurement Fock state	$\lvert\psi\rangle_{in} = \lvert 1\rangle$	$g_{34}^{(2)}(0)=1-\frac{1}{n}$; $g_{34}^{(2)}(0)=0$
7	Single-photon-interference	$\lvert\psi\rangle_{in} = \lvert 1\rangle$	We added this experiment as a supplement underscoring simultaneously two characteristics of the photon: The undividability and the ability of quantum randomness to interfere.

3.1 Calibration of the CCU: Coincidence window width *w*

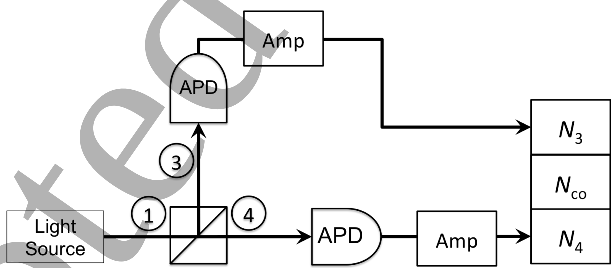

5 Outline of principle elements of the experimental set up

As shown in fig. 2 and 3 and described there, the shortened pulse occurs inside the solid state logic of the FPGA. Thus it is not possible to observe the w-pulse directly. To measure the coincidence window width w we determined $N_{34}(w)$, N_3 and N_4 for completely uncorrelated light of the LED with constant forward current (see fig. 5 for the principle set up). While expecting $g^{(2)}(0) = 1$, we can use eq. (2.5) to derive w from a linear fit:

$$\left.\begin{aligned} g_{3,4}^{(2)}(0) &= \frac{\langle N_3\cdot N_4\rangle_T}{\langle N_3\rangle_T\langle N_4\rangle_T} = \frac{\langle N_3\rangle_T\langle N_4\rangle_T}{\langle N_3\rangle_T\langle N_4\rangle_T} = 1 \\ g_{3,4}^{(2)}(0) &= \frac{N_{34}(w)}{\langle N_3\rangle_T\langle N_4\rangle_T}\frac{T}{w} \end{aligned}\right\} \Rightarrow \frac{N_{34}(w)}{\langle N_3\rangle_T\langle N_4\rangle_T} T = w = 2n\tau'. \quad (3.1)$$

The coincidence window width $w = 2 \cdot n \cdot \tau'$ could be adjusted by changing the number n of clock cycles (fig. 3). Fig. 6 shows the experimental results and a linear fit (eq. (3.2)) with parameters $\tau' = 2{,}45$ ns and $\Delta = 1{,}73$ ns:

$$\frac{N_{34}(w)}{\langle N_3\rangle_T \langle N_4\rangle_T} T = w = 2\tau' n + \Delta \tag{3.2}$$

The linearity between w and n is perfect ($R^2 = 1$). A reasonable origin of the intercept Δ is a slight increase of w not depending on the number of clock cycles due to a lowered slope of the leading edge of the measurement pulse (see fig. 4). For the following measurements we used the fitted value $w(n) = (4{,}90 \cdot n + 1{,}73)$ ns.

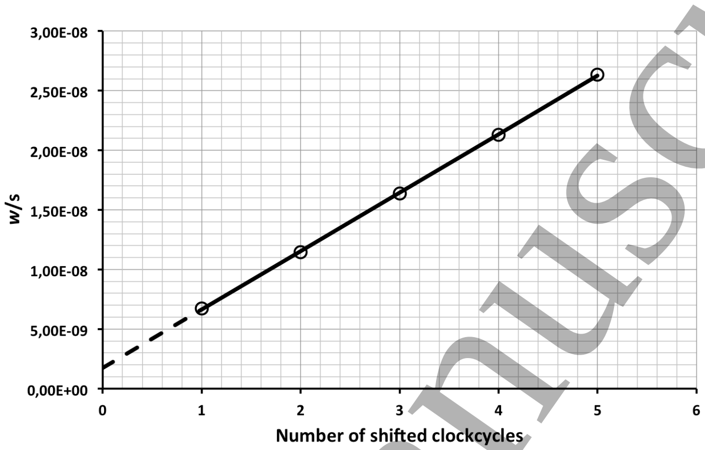

6 $w = T \cdot N_{34}(w)/(\langle N_3\rangle_T \cdot \langle N_4\rangle_T) = 2 \cdot n \cdot \tau' + \Delta$ as a function of the number n of clock cycles shifts (eq. (3.2))

3.2 Calibration of the CCU: Test of the coincidence-AND-gate-set-up

Our triple-gated scheme relies on the triple coincidence N_{34G} (eq. (2.7)) measured by a cascade of two AND gates. A small time delay of the input pulses is leading to counting losses in this gate cascade. This phenomenon seems to be typical for the measurement of triple coincidences and has been studied experimental carefully (see e. g. (Beck, 2007)). To check our system we used the triple detector set up shown in fig. 2 however with a piece of coloured fluorescence glass instead of the BBO-crystal and thus measuring solely accidental coincidences. Again scanning the window width $w(n)$ by varying the number n of clock cycles we get as a mean from 1.000 measurements (sampling time for each measurement 0.1 s):

n	$w(n)$/ns	N_G	N_3	N_4	N_{3G}	N_{4G}	N_{34}	N_{34G}	$g^{(2)}(0)$
1	6.64	390 387	164 596	165 958	432.97	422.25	180.23	0.390	0.835 (0.04)
2	11.54	394 050	164 005	168 712	739.43	788.80	324.01	1.199	0.810 (0.02)
3	16.44	401 140	169 879	172 790	1116,96	1129.72	478.08	2.457	0.781 (0.015)
4	21.35	395 900	160 767	170 826	1354,48	1469.36	589.571	3.874	0.771 (0.01)

Table I. Correlation results N_{34G} for the three output channels of the triple-gated scheme with uncorrelated fluorescence light from a coloured glass plate instead of the BBO-crystal (averaging over 1,000 runs); standard errors in parenthesis for $g^{(2)}$

n	$w(n)$/ns	N_G	N_3	N_4	N_{3G}	N_{4G}	N_{34}	N_{34G}	$g^{(2)}(0)$
1	6.64	390 387	164 596	165 958	432.97	422.25	180.23	0.488	1.045 (0.05)
2	11.54	394 050	164 005	168 712	739.43	788.80	324.01	1.501	1.014 (0.03)
3	16.44	401 140	169 879	172 790	1116,96	1129.72	478.08	3.074	0.977 (0.02)
4	21.35	395 900	160 767	170 826	1354,48	1469.36	589.571	4.848	0.964 (0.015)

Table II. Correlation results N_{34G} (corrected) for the three output channels of the triple-gated scheme with uncorrelated fluorescence light from a coloured glass plate instead of the BBO-crystal (averaging over 1,000 runs); standard errors in parenthesis for $g^{(2)}(0)$

The second order correlation function has been calculated from eq. (2.7) $g^{(2)}_{34\mathrm{G}} = \dfrac{N_{34\mathrm{G}} \cdot N_{\mathrm{G}}}{N_{3\mathrm{G}} \cdot N_{4\mathrm{G}}}$. Obviously $g^{(2)}(0)$ lies significantly below the value $g^{(2)}(0) = 1$, expected for uncorrelated light. From the measured values in table I we derive a mean correction factor 1/0.799 for $N_{34\mathrm{G}}$. Our further measurements will introduce this correction factor to avoid the gate-cascade-error in triple-coincidence experiments.

3.3 Measurement of light characteristics

Constant irradiance from a LED with constant forward current: $I(t) = \langle I \rangle = \text{const.}$

For completeness we report on this experiment from the calibration sequence. Here we used a 900-nm-infrared diode and a large sampling time $T = 100$ ms thus washing out any fluctuations. We can treat the irradiance as const. Fig. 7 shows the experimental results. We plotted the values of $g^{(2)}_{34}(0)$ for 2,000 single shots as a function of a increasing number of averaging steps:

$$\left\langle g^{(2)}_{34}(0) \right\rangle_M = \frac{1}{M} \sum_{l=1}^{M} g^{(2)}_{34}(0)_l ; 1 \le M \le 2000 . \tag{3.3}$$

It could be seen that $\left\langle g^{(2)}_{34}(0) \right\rangle_M$ approaches a value near the theoretical prediction $\lim\limits_{M\to\infty} \left\langle g^{(2)}_{34}(0) \right\rangle_M = g^{(2)}_{34}(0) = 1$.

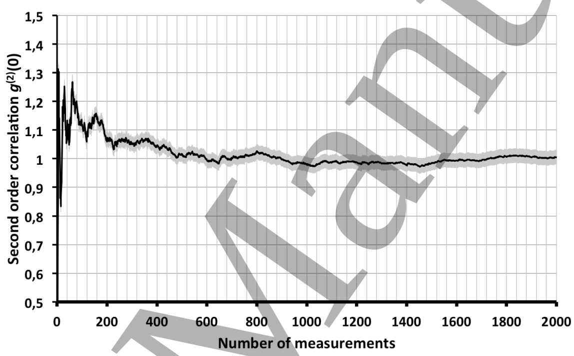

7 Light with constant irradiance approaching the value $g_{34}^{(2)}(0) = 1.02$ with increasing number of measurements. The theoretical prediction is $g_{34}^{(2)}(0) = 1$ (eq. (2.5). The shaded area shows the standard error.

Modulated irradiance: $I(t) = I_0 \cdot (1+S \cdot \sin\omega t)$

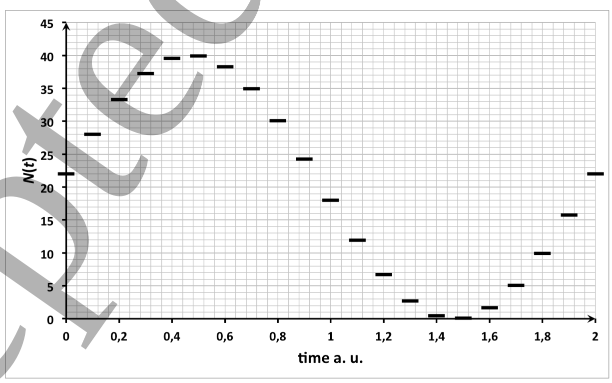

8 Left: The modulation of the irradiance, $N(t) = \eta I(t) T$

The next correlation experiment focuses on the situation of harmonically modulated irradiance $I(t) = I_0 \cdot (1+S \cdot \sin\omega t)$ with $|S| \le 1$ (fig. 8; this experiment has been proposed by Mark Fox in (Fox, 2006)). In the experiment we used a LED as light source with an appropriate modulated forward current and a detection sampling time ($T_1 \approx 100$ ms) long compared to the fluctuation time scale ($\approx 10^{-14}$ s). During a much longer detection period $T_2 \gg 1/\omega$ the sinusoidal modulated irradiance has been sampled.

The random fluctuations completely wash out during T_1 and with an excellent approximation the irradiance may treated constant during T_1: $I = I_0 = \text{const.}$ A standard function generator delivered the sinusoidal voltage signal to realize $0 < |S| \leq 1$. Gradually we varied the irradiance with a single step duration of $T_1 \approx 100$ ms. During each step the irradiance has been left unchanged (fig. 8). The steps almost follow the sin-function. For each step interval we take the irradiance as constant with the long time mean value of the irradiance $\langle I(t) \rangle = I_0$.

The second order correlation function is easily calculated for the modulated irradiance. From eq. (2.7) we get for a 50/50 beam splitter

$$g_{3,4}^{(2)}(0) = \frac{\langle I_3(t) I_4(t) \rangle_{T_2}}{\langle I_3(t) \rangle_{T_2} \langle I_4(t) \rangle_{T_2}} = \frac{\langle I(t)^2 \rangle}{\langle I(t) \rangle^2} = \frac{\left\langle \left(I_0 \left(1 + S \cdot \sin \omega t \right) \right)^2 \right\rangle_{T_2}}{\left\langle I_0 \left(1 + S \cdot \sin \omega t \right) \right\rangle_{T_2}^2}$$
$$= \left\langle \left(1 + S^2 \sin^2 \omega t \right) \right\rangle_{T_2} = 1 + \frac{1}{2} S^2. \tag{3.4}$$

The great advantage of this set up is a completely known temporal variation of the irradiance. Therefore this experiment gives a perfect introduction to $g^{(2)}(0)$-measurements and the usage of the CCU. Fig. 9 shows the joint presentation of the experimental results and the theoretical expectation for $T = 100$ ms and $w(n = 2) = (2 \cdot 4{,}90 + 1{,}73)$ ns. The excellent agreement between theory and experiment is disturbed by a discrepancy for higher S-values. This discrepancy is caused by an interesting noise phenomenon: For high modulation amplitudes the low irradiance part of $I(t) = I_0 \cdot (1 + S \cdot \sin \omega t)$ reaches the dark noise area of the APD (dark noise clipping).

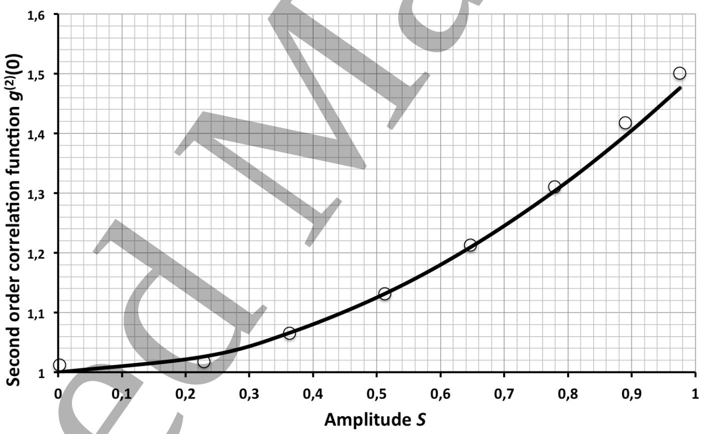

9 The second order coherence function $g^{(2)}(0)$ as a function of the modulation amplitude S; open circles experimental values, closed line directly eq. (3.13) resp. 4.4. The standard error is much smaller than the diameter of the circles.

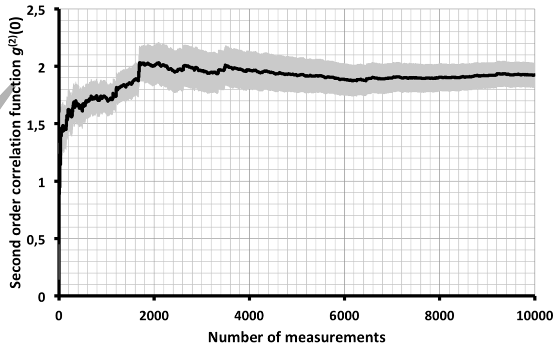

10 $g^{(2)}(0) \rightarrow 1.93$ for pseudo thermal light. The theoretical prediction is $g^{(2)}(0) = 2$. The shaded area shows the value of the standard error.

(Pseudo-) thermal light: $I(t) = \langle I \rangle + \Delta I_{th}$; N geometrically distributed

Here we analysed the light from the (pseudo-) thermal modulated LED recently published (Scholz et al., 2016). To apply eq. (2.5) the mean values of $g^{(2)}(0)$ has been calculated by averaging over 10,000 measurements. Fig. 10 demonstrates the process of approaching the final values of $g^{(2)}(0)$. After 10,000 shots we found $g^{(2)}(0) \to 1.93$ (fig. 10), a value in good agreement with the theoretical value $g^{(2)}(0) = 2$ (see eq. (B.4)).

Single photon quantum light at the beam splitter

For a quantum physical perspective the classical light field strength has to be replaced by the appropriate quantum physical operators (see introductory quantum optics textbooks, e.g. Grynberg, Aspect & Fabre, 2010). For a single mode field we get:

$$E(t) = E_0(t)\sin(\omega t - kz) \propto \mathrm{i}\left(\alpha \exp \mathrm{i}kz - \alpha^* \exp - \mathrm{i}kz\right) \to$$
$$\hat{E}(t) \propto \mathrm{i}\left(\hat{a} \exp \mathrm{i}kz - \hat{a}^\dagger \exp - \mathrm{i}kz\right),$$

with the quantum mechanical ladder operators $\hat{a}^\dagger$ for the creation of a photon and $\hat{a}$ for the annihilation of a photon. The number of photons in the quantum optical light state is counted by the number operator $\hat{n} = \hat{a}^\dagger \cdot \hat{a}$.

From a quantum optical calculation of the correlation function (see appendix B) we can deduce theoretical values for $g^{(2)}(0)$. For this purpose we have to replace the classical numbers like $\langle N_3 \cdot N_4 \rangle$ in eq. (2.4) by appropriate quantum mechanical number operators $n \to \hat{n}$:

$$g^{(2)}_{3,4}(0) = \frac{\langle N_3 N_4 \rangle}{\langle N_3 \rangle \langle N_4 \rangle} \to g^{(2)}_{3,4}(0) = \frac{\langle \hat{n}_3 \hat{n}_4 \rangle}{\langle \hat{n}_3 \rangle \langle \hat{n}_4 \rangle}. \quad (3.5)$$

Here we can use the number of photons instead of the number of photoelectrons from the detector. Due the gated single photon set up the number of photoelectrons from the binary detector and the number of photons are identical.

With a little operator algebra (see appendix B) eq. (3.5) can be traced back to the number of photons at the input of the beam splitter characterizing the input light

$$g^{(2)}_{34}(0) = \frac{\langle \hat{n}_3 \hat{n}_4 \rangle}{\langle \hat{n}_3 \rangle \langle \hat{n}_4 \rangle} = 1 + \frac{\mathrm{var}(n_1) - \langle n_1 \rangle}{\langle n_1 \rangle^2}. \quad (3.6)$$

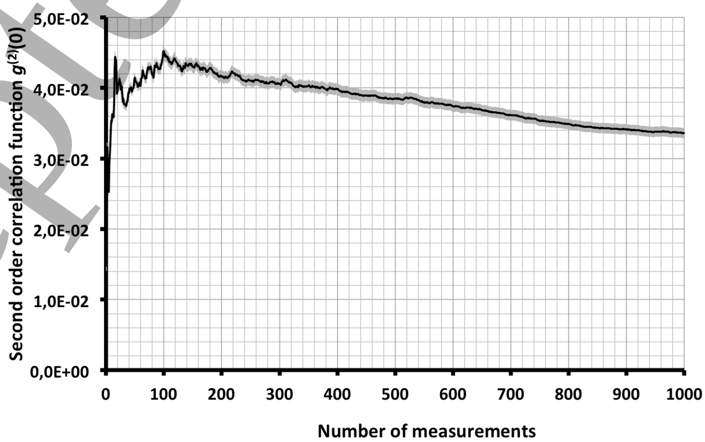

11 $g^{(2)}(0)$ for single photon light approaching the value $g^{(2)}(0) \ll 1$ with increasing number of measurements. The theoretical prediction is $g^{(2)}(0) = 0$ (eq. (B.4)). The shades area shows the standard error. Residual accidental 3-fold coincidences and residual dark noise from the detectors lead a lower limit $g^{(2)}(0) > 0$.

By definition Fock photon states do not exhibit variances of the photon number: var(n) = 0. Thus Eq. (3.6) yields $g_{34}^{(2)}(0)=0$. The experimental results are shown in fig. 11: $g_{34}^{(2)}(0)\ll 1$. The dramatic loss of correlation is usually called antibunching. This phenomenon has been first published by Mandel and co-workers (Kimble, Dagenais, & Mandel, 1977). Since then an overwhelming bunch of literature deals with this quantum effect. We included the phenomenon not only to demonstrate the functional capability of the set up in a more advanced experimental region closer to research. It seems to be obvious that antibunching experiments work as key experiments in a contemporary introduction to quantum physics. And according to this educational feature this experiment serves as a obvious completion of our experimental steps to quantum physics.

Stochastic of photons

With our experiments it was unequivocally established that no (or virtually no; take special notice of the ordinate scaling) coincidence between output channels D_3 and D_4 can be measured. Photons are passing the beam splitter without being divided. This experiment clearly violates the predictions holding for any classical wave model. It should be noted that on the other hand the nonlinear PDC-process itself may be viewed as a perfect beam splitter, even suited to split the incoming photon into two perfectly correlated ones coming out off the nonlinear crystal. Our arguments however focus on linear optical devices where photon splitting is not possible.

An interesting perspective arises if one keeps in mind that the unitary transformation from the beam splitter can not be the origin of randomness. The output state of the beam splitter is a deterministic superposition of the two possible output channels ($\frac{1}{\sqrt{2}}\left(|0\rangle_3|1\rangle_4+|1\rangle_3|0\rangle_4\right)$). Under this perspective the randomness arises due to the detection. Complete *decoherence (a quantum-to-classical-transition) of the superposition* occurs due to the interaction of the photon and the detector. Finally one of the detectors annihilates the photon by measuring it and thus slurring the whole photon energy. The other detector will never be able to coincide (Leuchs, G., 2016).

Photons "between a rock and a hard place"

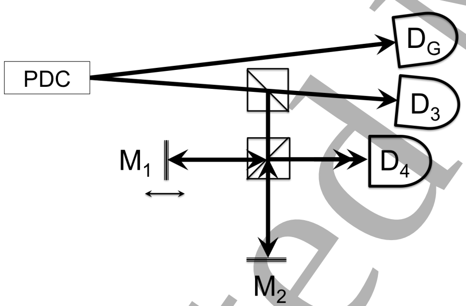

12 Two different quantum features in one experiment: At the first beam splitter photons behave like particles following a 0.5-probability to be reflected into the interferometer; there photons show the interference of quantum mechanical randomness.

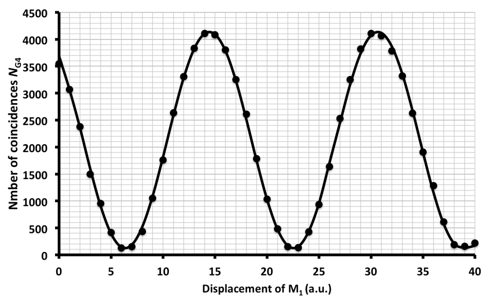

13 Two-fold coincidences N_{4G} for the single photons show perfect fringes of the interference pattern (visibility V = 93 %); dashed curve shows the $\cos^2$-fit; the standard error of the measurement is of the order of the diameter of the closed circles

This experiment is designed to reveal the photon's two sides of the same coin. A rough sketch of the experimental set up is shown in fig. 12. At the first beam splitter photons are reflected with a 0.5-probability. The two output channels (transmission vs. reflection) show the $g^{(2)}(0)$ = 0-antibunching of undividable photons (fig. 11). Now it follows a Michelson interferometer. A single photon interacts with the Michelson producing interference. Scanning the distance between mirror M_1 and the beam splitter we find a perfect interference pattern with 93% visibility (s. fig. 13). What is the origin of an interference if there is no wave? At this point we open the door to quantum physics arguments dealing with one of the special feature of quantum physics: The ability of quantum probability to interfere (Heusler & Schlichting, 2005).

The origin for a lower limit $N_{4G,\,min} > 0$ is the sum of noise effects: Thermal noise from the APD, electronic noise from the power device, vibrations of the set up.

4 Conclusion

We demonstrated a series of undergraduate experiments designed to pave the way to quantum optics.

- Fluctuations of light with constant irradiance should be embedded into a discussion of both, the Poissonian produced by the binary detector and as a consequence of discrete occurrence of undividable photons.
- Modulated irradiance gives a very easy access to $g^{(2)}$-analysis without oversimplifying the subject. This experiment is well suited to introduce the complete stochastic tool box used around fluctuation measurement schemes.
- The observation of fluctuations of thermal light yields very fast detectors. On the other hand the production of (pseudo-) thermal light via the appropriate controlling of the forward current of a LED is pretty easy and is leading to particularly suited undergraduate experiments: Experiments showing bunching-phenomena in statistical optics may surely be viewed as milestone experiments on the way to antibunching experiments in quantum optics.
- Finally the single-photon-experiments show as well the special meaning of real single-photons (unlike low irradiance of laser light), it demonstrates kernel characteristics of quantum physics that cannot be described by classical physics (superposition, interference of the single-photon state).

All these experiments rely on fluctuation phenomena. The theoretical difference between classical physics and photon-quantum-mechanics is comprehensible and closely squired by appropriate experiments. Thus our experiments are well suited for an experimental based approach to quantum physics. They are designed to avoid photon-misconceptions, to reduce relevant access-barriers and hopefully tends to open student's minds for completely new physical concepts. Undergraduate quantum optics experiments have been published previously and have been successfully used in undergraduate labs (Thorn et al. 2004). The special idea behind the way presented in this paper is targeting on a particular focussed training of statistical optical methods relying on $g^{(2)}$-measurements before entering the quantum world. The usage of correlation measurements will not produce major difficulties at university. To open the door of classrooms at school for a correlation analysis, however we will have to invest much more into teacher's training, in service and before.

Next steps: The observation of polarization entangled photonic states and an appropriate Bell-analysis will integrate another central quantum feature into the course. Careful studies of noise should reveal sub-Poissonian behaviour for the entangled photon states, provided the quantum efficiency of the APD is high enough.

Further reading: The physics of single photon light is the topic of numerous publications. From this overwhelming bunch we would like to recommend three publications that seem to be well suited to support undergraduate studies:

- Antibunching of single photons and the method of photon counting at a beam splitter has been demonstrated in a particularly cogent way in (Grangier, Roger, and Aspect, 1986). Though experimentally not easy to handle, the fluorescence cascade exhibits a quite high level of clarity.
- In a different experimental set up two distinct quantum features could be observed simultaneously: The fluorescence light from a single stored atomic ion in a radiofrequency trap shows antibunching (proofed by a $g^{(2)}$-analysis of coincident signals) and a probability distribution significant narrower than Poissonian (Diedrich and Walther, 1987).
- A clarifying spot on experiments with single photons and beam splitters and a virtually complete list of the relevant literature could be found in the ICO Newsletter 106, January 2016 "Getting used to quantum optics ... " (Leuchs, 2016).

Acknowledgements

The authors wish to thank Prof. Jan-Peter Meyn for valuably supporting the development of the experimental set up incl. the APD-detector scheme. The authors also acknowledge financial support from the SFB 1227/DQ-*mat* and the Leibniz Universitaet Hannover. And finally we wish to express our sincere thanks to the reviewers. Their detailed constructive remarks helped to realize a considerable improvement from the first draft to the final version of this paper.

References

Beck, M. (2007). Comparing measurements of $g^{(2)}(0)$ performed with different coincidence detection techniques. *J. Opt. Soc. Am., 24*(12), 2972–2978.

Branning, D., Bhandari, S., & Beck, M. (2009). Low-cost coincidence-counting electronics for undergraduate quantum optics. *Am. J. Phys.*, *77*(7), 667–670.

Dhulla, V. H. (2007) *Single Photon Counting for Ultra-weak Fluorescence Detection: System Design, Characterization and Application to DNA-sequencing.*Diss. Stony Brook University

Diedrich, H. and Walther, H. (1987). Nonclassical radiation of a single stored ion. *Phys. Rev. Let.* 58, 203–206

Eckart, C., & Shonka, F. R. (1938). Accidental coincidences in counter circuits. *Phys. Rev.*, *53*(9), 752–756.

Fox, M. (2006). *Quantum Optics* (Second Edition). Oxford: Oxford University Press.

Galvez, E. J., & Beck, M. (2007). Quantum Optics Experiments with Single Photons for Undergraduate Laboratories. *Proc. SPIE 9665,* Tenth International Topical Meeting on Education and Training in Optics and Photonics, 966513-1–966513-7; doi: 10.1117/12.2207351

Glauber, R. J., (1963). Coherent and incoherent states of radiation field. *Phys. Rev.* (*131*) 2766–2788

Goodman, J. W. (1976). Some fundamental properties of speckle. *J. Opt. Soc. Am.*, *66*(11), 1145.

Goodman, J. W. (2000). *Statistical Optics.* Wiley Classics Library Edition, John Wiley & Sons, first published 1985

Grangier P., Roger G., Aspect A., (1986), Experimental Evidence for a Photon Anticorrelation Effect on a Beam Splitter: A New Light on Single Photon Interferences. *Europhys. Lett. 1*, 173–179

Grynberg, G., Aspect, A., and Fabre, C. (2010). *Introduction to Quantum Optics*. Cambridge University Press

Hanbury Brown, R. and Twiss, R. Q. (1956). Correlation between photons in two coherent beams of light. *Nature, 177*, 27

Heusler, S. and Schlichting, J. (2005). Interferenz von Wahrscheinlichkeiten. *phydid A, 1/7,* 9–14

Kimble, H. J., Dagenais, M., and Mandel, L. (1977). Photon Antibunching in Resonance Fluorescence. *Phys. Rev. Lett. 39(11)*, 691

Leuchs, G. (2016). Getting used to quantum optics ... *ICO Newsletter 106*

Loudon, R. (2000). *The Quantum Theory of Light* (Third Edit). Oxford: Oxford University Press.

Mandel, L. (1958). Fluctuations of Photon Beams and their Correlations. *Proc. Phys. Soc.*, *72*(6), 1037–1048.

Pearson, B. J., & Jackson, D. P. (2010). A hands-on introduction to single photons and quantum mechanics for undergraduates. *Am. J. Phys.*, *78*(5), 471–484.

Saleh B. (1978). *Photoelectron Statistic*. Berlin Heidelberg New York: Springer Series in Optical Sciences

Scholz, R., Friege, G., & Weber, K.-A. (2016). Undergraduate experiments on statistical optics. *Europ. J. Phys.*, *37*(5), 55302.

Thorn, J. J., Neal, M. S., Donato, V. W., Bergreen, G. S., Davies, R. E., and Beck, M., (2004). Observing the quantum behavior of light in an undergraduate laboratory. *Am. J. Phys., (72)*, 1210–1219

Appendix A Mean and variance

Typical results of counting experiments using binary Geiger mode detectors are probability distributions, mean values and variances of impulses processes from the detector. The connection between the irradiance of the incoming light and the count statistics is of vital importance. For a lot of cases this connection can be described by a Poissonian impuls process. A mean irradiance (see eq. (2.1)) impinging on the detector during time T leads to a mean value of $\left\langle N\right\rangle_T = \eta T\left\langle I(t)\right\rangle_T$ counts. The probability to get N counts is given by (Loudon, 2000)

$$P_T(t,N) = \frac{\left(\eta T\left\langle I(t)\right\rangle_T\right)^N}{N!}\exp\left(-\eta T\left\langle I(t)\right\rangle_T\right). \tag{A.1}$$

Mean and variance from Mandel's formula

The experiments are usually performed as series of independent "single shots". The final result is in those cases the mean value averaged over all measurements:

$$P_T(M) = \left\langle \frac{\left(\eta T\left\langle I(t)\right\rangle_T\right)^M}{M!}\exp\left(-\eta T\left\langle I(t)\right\rangle_T\right)\right\rangle_{\text{measurements}}. \tag{A2}$$

This formula is often referred to as Mandel's formula (Mandel,1958). Starting with eq. (A.2) the calculation of the mean value and the variance is straight forward:

$$\begin{aligned}\left\langle N\right\rangle &= \sum_{M=0}^{\infty} M P_T(M) = \left\langle \sum_{M=0}^{\infty} M\frac{\left(\eta T\left\langle I(t)\right\rangle_T\right)^M}{M!}\exp\left(-\eta T\left\langle I(t)\right\rangle_T\right)\right\rangle \\ &= \left\langle \left(\eta T\left\langle I(t)\right\rangle_T\right)\underbrace{\sum_{M=1}^{\infty}\frac{\left(\eta T\left\langle I(t)\right\rangle_T\right)^{M-1}}{(M-1)!}\exp\left(-\eta T\left\langle I(t)\right\rangle_T\right)}_{1}\right\rangle = \left\langle \eta T\left\langle I(t)\right\rangle_T\right\rangle.\end{aligned} \tag{A3}$$

$$\begin{aligned}\left\langle N^2\right\rangle &= \sum_{M=0}^{\infty} M^2 P(M) = \left\langle \sum_{M=0}^{\infty} M^2\frac{\left(\eta T\left\langle I(t)\right\rangle_T\right)^M}{M!}\exp\left(-\eta T\left\langle I(t)\right\rangle_T\right)\right\rangle \\ &= \left\langle \eta T\left\langle I(t)\right\rangle_T \sum_{M=1}^{\infty} M\frac{\left(\eta T\left\langle I(t)\right\rangle_T\right)^{M-1}}{(M-1)!}\exp\left(-\eta T\left\langle I(t)\right\rangle_T\right)\right\rangle \\ &= \left\langle \eta T\left\langle I(t)\right\rangle_T\left(\underbrace{\sum_{M=1}^{\infty}\frac{\left(\eta T\left\langle I(t)\right\rangle_T\right)^{M-1}}{(M-1)!}\exp\left(-\eta T\left\langle I(t)\right\rangle_T\right)}_{=1} + \sum_{M=1}^{\infty}(M-1)\frac{\left(\eta T\left\langle I(t)\right\rangle_T\right)^{M-1}}{(M-1)!}\exp\left(-\eta T\left\langle I(t)\right\rangle_T\right)\right)\right\rangle \\ &= \left\langle \eta T\left\langle I(t)\right\rangle_T\left(1+\eta T\left\langle I(t)\right\rangle_T\underbrace{\sum_{M=2}^{\infty}(M-2)\frac{\left(\eta T\left\langle I(t)\right\rangle_T\right)^{M-2}}{(M-2)!}\exp\left(-\eta T\left\langle I(t)\right\rangle_T\right)}_{=1}\right)\right\rangle \\ &= \left\langle \eta T\left\langle I(t)\right\rangle_T + \left(\eta T\left\langle I(t)\right\rangle_T\right)^2\right\rangle = \left\langle N\right\rangle + \left\langle\left(\eta T\left\langle I(t)\right\rangle_T\right)^2\right\rangle.\end{aligned} \tag{A4}$$

Thus we get the variance of the count number N:

$$\mathrm{var}(N) = \langle N^2 \rangle - \langle N \rangle^2 = \langle N \rangle + \left\langle \left(\eta T \langle I(t) \rangle_T \right)^2 \right\rangle - \left\langle \left(\eta T \langle I(t) \rangle_T \right) \right\rangle^2 . \tag{A5}$$

The first term is the contribution from the Poissonian character of the binary detector's single shot regime (shot noise), independent on the light features, while second one is contributed by the physical characteristics of the light fluctuations.

Photo counts from coherent laser light

In some cases the averaging process in eq. (A.2) can be carried out by an integration over the distribution $p(i)\mathrm{d}i$ of the irradiance (see Goodman 2000):

$$\begin{aligned} P_T(M) &= \left\langle \frac{\left(\eta T \langle I(t) \rangle_T \right)^M}{M!} \exp\left(-\eta T \langle I(t) \rangle_T \right) \right\rangle_{\text{measurements}} \\ &= \int_0^\infty \mathrm{d}\langle I(t) \rangle_T \, p\left(\langle I(t) \rangle_T \right) \frac{\left(\eta T \langle I(t) \rangle_T \right)^M}{M!} \exp\left(-\eta T \langle I(t) \rangle_T \right). \end{aligned} \tag{A.6}$$

For ideal laser light the irradiance I_0 is constant and the distribution is given by Dirca's delta function $p(i)\mathrm{d}i = \delta(i - I_0)\, \mathrm{d}i$. The count numbers are Poisson distributed in this case ($i = \langle I(t) \rangle_T$)

$$\begin{aligned} P_T(M) &= \int_0^\infty \mathrm{d}i \delta\left(i - I_0 \right) \frac{(\eta T i)^M}{M!} \exp(-\eta T i) \\ &= \frac{(\eta T I_0)^M}{M!} \exp(-\eta T I_0). \end{aligned} \tag{A.7}$$

Photo counts from thermal light

For polarized thermal light the irradiance could be shown to be exponential distributed (Goodman, 2000), $p(i)\mathrm{d}i = \frac{1}{\bar{I}} \exp\left(-{}^{i}\!/\!_{\bar{I}} \right)$, with a long time mean for the irradiance $\bar{I}$. Inserting into eq. (A.2) the distribution of counts is evaluated as

$$\begin{aligned} P_T(M) &= \frac{1}{\bar{I}} \int_0^\infty \mathrm{d}i \exp\left(-\frac{i}{\bar{I}} \right) \frac{(\eta T i)^M}{M!} \exp(-\eta T i) \\ &= \frac{(\eta T)^M}{\bar{I} M!} \int_0^\infty \mathrm{d}i (\eta T i)^M \exp\left(-i \left(\frac{\eta T \bar{I} + 1}{\bar{I}} \right) \right) \\ &= \frac{(\eta T)^M}{\bar{I} M!} \frac{\bar{I}^{M+1} M!}{(\eta T \bar{I} + 1)^{M+1}} = \frac{\langle M \rangle^M}{\left(\langle M \rangle + 1 \right)^{M+1}}. \end{aligned} \tag{A.8}$$

With a long time mean for the count number $\langle M \rangle = \eta T \bar{I}$ and $\int_0^\infty \mathrm{d}x x^n \exp(-ax) = {}^{n!}\!/\!_{a^{n+1}}$.

Thermal light photon distribution

As shown in many quantum optics textbooks the probability distribution of the photon number n, the mean values $\langle n \rangle$ and the var(n) can be calculated directly from Planck's formula. Starting with the definition of the expectation value we get for a single radiation mode within a cavity in the thermal equilibrium (with an absolute temperature T):

$$
\begin{aligned}
&P(n) = \left(1-\exp\left(-\hbar\omega / k_{\mathrm{B}}T\right)\right)\cdot\exp\left(-n\hbar\omega / k_{\mathrm{B}}T\right) = (1-U)U^{n}\\
&\langle n\rangle = \sum_{n=0}^{\infty} P(n)\,n = (1-U)\sum_{n=0}^{\infty} U^{n} n\\
&\langle n^{2}\rangle = \sum_{n=0}^{\infty} P(n)\,n^{2} = (1-U)\sum_{n=0}^{\infty} U^{n} n^{2}
\end{aligned}
\tag{A.9}
$$

Now applying the helpful differentiating procedure to evaluate the sum (e. g. Fox 2006) we get

$$
\begin{aligned}
\langle n\rangle &= \sum_{n=0}^{\infty} P(n)\,n = (1-U)\sum_{n=0}^{\infty} U^{n} n = (1-U)U\frac{\mathrm{d}}{\mathrm{d}U}\sum_{n=0}^{\infty} U^{n}\\
&= (1-U)U\frac{\mathrm{d}}{\mathrm{d}U}\frac{1}{1-U} = (1-U)U\frac{1}{(1-U)^{2}} = \frac{1}{U^{-1}-1}\\
\langle n\rangle &= \frac{1}{\exp\left(\hbar\omega / k_{\mathrm{B}}T\right)-1}.
\end{aligned}
\tag{A.10}
$$

$$
\begin{aligned}
\langle n^{2}\rangle &= \sum_{n=0}^{\infty} P(n)\,n^{2} = (1-U)\sum_{n=0}^{\infty} U^{n} n^{2} = (1-U)\sum_{n=0}^{\infty} nU^{n} + U^{2}\frac{\partial^{2}}{\partial U^{2}}U^{n}\\
&= \langle n\rangle + 2\left(\frac{U}{1-U}\right)^{2} = \langle n\rangle + 2\langle n\rangle^{2}.
\end{aligned}
\tag{A.11}
$$

$$
\operatorname{var}(n) = \langle n^{2}\rangle - \langle n\rangle^{2} = \langle n\rangle + 2\langle n\rangle^{2} - \langle n\rangle^{2} = \langle n\rangle + \langle n\rangle^{2}.
\tag{A.12}
$$

Appendix B Derivation of the quantum version of $g^{(2)}(0)$

For a quantum field we merely replace the classical averages like $N_{34} = \langle N_3 \cdot N_4\rangle$ by the appropriate quantum mechanical operators. The first step is to introduce the number operators: $n \rightarrow \hat{n} = \hat{a}^{\dagger}\hat{a}$. $\hat{a}^{\dagger}$ and $\hat{a}$ are the operators, raising and lowering the number of photons by 1, respectively:

$$
\left.\begin{aligned}
\hat{a}|n\rangle &= \sqrt{n}\,|n-1\rangle\\
\hat{a}^{\dagger}|n\rangle &= \sqrt{n+1}\,|n+1\rangle
\end{aligned}\right\}\Rightarrow\left\{\begin{aligned}
\hat{a}^{\dagger}\hat{a}|n\rangle &= \hat{a}^{\dagger}\sqrt{n}\,|n-1\rangle = n|n\rangle\\
\hat{a}\hat{a}^{\dagger}|n\rangle &= \hat{a}\sqrt{n+1}\,|n+1\rangle = (n+1)|n\rangle
\end{aligned}\right.
\tag{B.1}
$$

The effect of lossless beam splitters is usually described by a unitary transformation relating the output fields to the input fields classically and quantum mechanically as well. The particular form of the transformation matrix depends on a phase difference between the transmitted and reflected photon wave function (Loudon, 2000). One of the most simplest relations is given by

$$
\begin{pmatrix} a_3^{\dagger} \\ a_4^{\dagger} \end{pmatrix} = \frac{1}{\sqrt{2}}\begin{pmatrix} 1 & 1 \\ 1 & -1 \end{pmatrix}\begin{pmatrix} a_1^{\dagger} \\ a_2^{\dagger} \end{pmatrix}.
\tag{B.2}
$$

Now, with eq. (B.1) and inserting the commutator rule for ladder operators: $\left[\hat{a},\hat{a}^{\dagger}\right] = \hat{a}\cdot\hat{a}^{\dagger} - \hat{a}^{\dagger}\cdot\hat{a} = 1$ we finally get the number operators for the two beam splitter output channels D_3 and D_4. Evaluating eq. (B.2) we used the fact, that in quantum optics "no light at input 2" means "the vacuum state $|0\rangle$ is coupled to input 2". Now we can use eq. (B.1) with $\hat{a}_2|0\rangle = \langle 0|\hat{a}_2^{\dagger} = 0$ to get rid of the $\hat{a}_2$ -terms:

$$
\begin{aligned}
\hat{n}_3\hat{n}_4 &=: \hat{a}_3^\dagger \hat{a}_3 \hat{a}_4^\dagger \hat{a}_4 : \\
&= \hat{a}_3^\dagger \hat{a}_4^\dagger \hat{a}_3 \hat{a}_4 \\
&= \frac{1}{4}\left(\hat{a}_1^\dagger + \hat{a}_2^\dagger\right)\left(\hat{a}_1^\dagger - \hat{a}_2^\dagger\right)\left(\hat{a}_1 + \hat{a}_2\right)\left(\hat{a}_1 - \hat{a}_2\right) = \frac{1}{4}\hat{a}_1^\dagger\left(\hat{a}_1^\dagger - \hat{a}_2^\dagger\right)\left(\hat{a}_1 + \hat{a}_2\right)\hat{a}_1 \\
&= \frac{1}{4}\hat{a}_1^\dagger \hat{a}_1^\dagger \hat{a}_1 \hat{a}_1 = \frac{1}{4}\left(\hat{a}_1^\dagger \hat{a}_1 \hat{a}_1^\dagger \hat{a}_1 - \hat{a}_1^\dagger \hat{a}_1\right) = \frac{1}{4}\hat{n}_1\left(\hat{n}_1 - 1\right).
\end{aligned}
\tag{B.3}
$$

By means of eq. (B.3) we evaluate the quantum mechanical second order correlation function (see also Roy Glauber's original publication for additional details (Glauber, 1963)). The ordering of the operators between colons (:…:) is referred to as normal ordering: Gathering all creation operators on the left side while the annihilation operators are ordered to the right side. With eq. (B.3) inserted into eq. (B.1) we finally find for the second order correlation function

$$
\begin{aligned}
g_{3,4}^{(2)}(0) &= \frac{\langle N_3 N_4\rangle}{\langle N_3\rangle\langle N_4\rangle} \to \frac{\langle \hat{n}_3\hat{n}_4\rangle}{\langle \hat{n}_3\rangle\langle \hat{n}_4\rangle} \\
&= \frac{\langle \hat{n}_1\left(\hat{n}_1 - 1\right)\rangle}{\langle \hat{n}_1\rangle^2} = \frac{\langle \hat{n}_1^2 - \hat{n}_1\rangle}{\langle \hat{n}_1\rangle^2} = 1 + \frac{\mathrm{var}\left(n_1\right) - \langle n_1\rangle}{\langle n_1\rangle^2} \\
&= \begin{cases} 1 \text{ for Poissonian light with } \mathrm{var}\left(n_1\right) = \langle n_1\rangle \\ 2 \text{ for thermal light with } \mathrm{var}\left(n_1\right) = \langle n_1\rangle + \langle n_1\rangle^2 \\ 1 - \dfrac{1}{\langle n_1\rangle} \text{ for quantum optical Fock-light with } \mathrm{var}\left(n_1\right) = 0 \end{cases}.
\end{aligned}
\tag{B.4}
$$

Two remarks for clarification: (1) Quantum mechanics enter the formal argumentation via the commutation relation of the destruction and creation operators in eq. (B.1). (2) Antibunching relying on the ability of single photon interference as a specific quantum aspect of the photon solely occurs in a quantized treatment. (3) For single photon experiment we get $g^{(2)}{}_{3,4}(0) = 0$.

Appendix C Apparatus Notes

Fig. C.1 shows a photo of the experimental set up. Here we give some technical details of the apparatus used in the experiments.

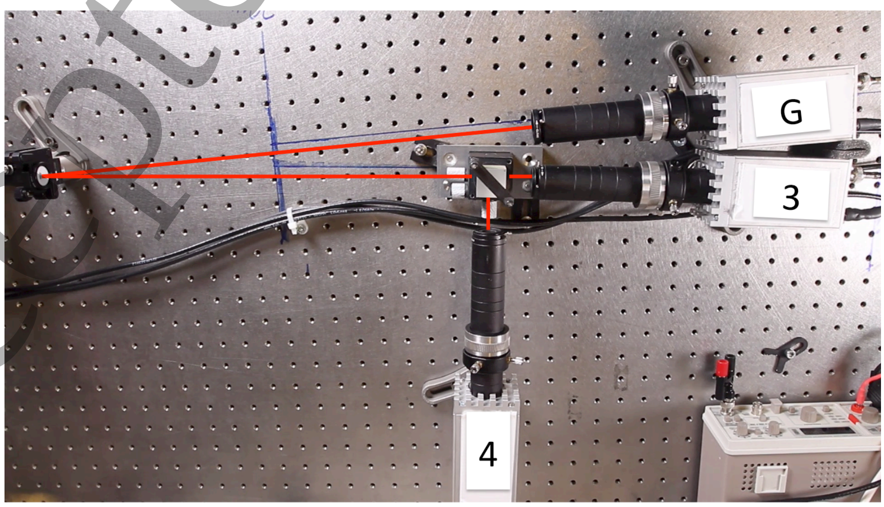

C.1 Experimental set up for the single photon experiment; the light beams are highlighted

The pump-laser

We used a GaN based laser-diode (Sanyo DL-4146-101S) without external cavity. Active Peltier-stabilization of the temperature to ± 1mK yields a peak-wavelength stabilized to approximately ± 0.1 pm. The optical power P could been controlled via a stabilized forward current of the diode in the range 22 mA $\leq I_{\text{diode}} \leq$ 35 mA leading to an optical power range 0.1 mW $\leq P \leq$ 15 mW. From a Gaussian fit we found an oval shaped beam crosssection with diameters D_x/D_y = (1.032 ± 0.012) mm/(1.260 ± 0,012) mm at the location of the BBO-cristal (see fig. C.2).

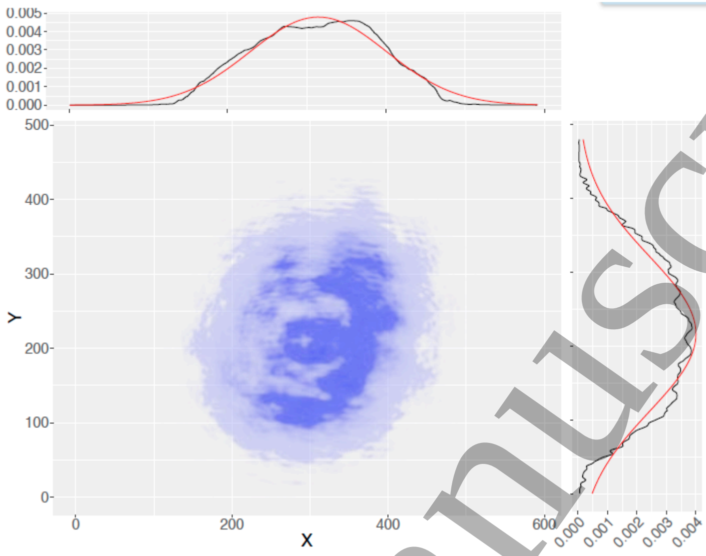

C.2 Measurement of the beam crosssection; from the Gaussian fit we get (1.032 ± 0.012) mm/(1.260 ± 0,012) mm

Linear polarization of the laser radiation has been ensured via external polarizing filters.

The nonlinear crystal

For the type-1 parametric-down-conversion we used a coated BBO-crystal sized $W = H = 6$ mm; $L = 3$ mm; (BBO-0805-23H-crystal from Eksma Optics) with 29.2°-cutting-angle; input wavelength 405 nm, output wavelength 810 nm.

Detector system

Summarizing the technical demands for our high speed low light level APDs

- not fiber based (for didactical reasons)
- high quantum efficiency in the near IR (810 nm)
  at 810 nm we could realize a quantum efficiency of about 80 %
- small dead time to avoid a nonlinear response in the case of high photon rates
  the APD-dead time of τ_D = 50 ns is given by the length of the quenching pulse; it follows an upper limit of the photon counting rates much below $1/\tau_D = 20 \cdot 10^6\ \text{s}^{-1}$
- immunity against overexposure
  to minimize the risk to destroy the detector diode by high avalanche currents, we used an electronic protection circuit similar to the one used by (Dhulla, 2007)
- electrical safety
  educational use imposes high safety demands. The detection system follows CE-standards (e. g. a housing connected to PE)

Counting unit

The coincidence counting unit is central for the correlation analysis within the photon counting experiments. The general mode of operation is represented in section 2.4.

In our setup we have to meet following technical requirements:

- based on electronics easy to combine and understand
- at least three channels to measure 3-fold coincidence
- a 24-bit counter with sampling rate well above 10^6 s^{-1}
- precise controlling of the sampling time T
- a smallest possible coincidence window width of $w < 7$ ns
- a variably adjustable coincidence window width w
- live visualization of the measurements on a Host-system
- precisely defined number of single shots for each measurement (see eq. (2.2))

Due to the demands of a multiplication of the experimental set ups for the utilization in an educational lab, the costs are limited to 300 € per counting unit.

The counting unit consists of four subunits: A level-shifter converting the incoming TTL pulse to a logic level of 3.3 V (20 €), a FPGA on the Altera DE0-nano evaluation board (100 €), a 40 Pin to 40 Pin remapping pcb (15 €) adapting outputs of the FPGA to the inputs of the last subunit a Raspberry Pi 3 acting as host-system (50 €, including power-supply and sd-card for the operating system). The system is housed in a lasercutted acrylic box (35 €). We end up with a price of 220 €.

The level-shifter:

Operating voltage of the FPGA is 3.3 V, therefore a conversion of the incoming signal is needed. The level-shifter converts incoming 5 V-high-level-pulses to 3.3 V. This is done with a 74LVX244 octal buffer actively, which is fast enough. With advanced experiments in view, the design has been expanded to a four input channel system.

The FPGA:

Field Programmable Gate Arrays (FPGA) are designed for parallel-data-processing, thus they may be used to drive several counter-instances simultaneously. Expanding the system to a parallel driving of 15 counter aimed to open up additional counting opportunities: One for each input channel (4), six for the 2-fold coincidences (6), four for the 3-fold coincidences (4) and one for the 4-fold coincidences (1). Moreover the pulse-shorter and pulse-ANDer are units realized on the FPGA. The FPGA is programmed in Verilog Hardware Description Language (VHDL) (source-code can be requested from the authors). We use the implementation of the FPGA on an evaluation board to get an out of the box running system at reasonable expanse and value.

The 40 pin-40 pin remapping:

The 40 pin-header of the Altera DE0-Nano board is incompatible to that one of the Raspberry PI. Therefore a remapping is needed. Instead of doing this with a reordered broadband cable, a remapping pcb was designed. Easy and fast replication of the hole system is given.

The host-system:

The host-system provides a graphical user interface (gui) for setup the counting unit (sampling time, coincidence time in steps of 6.6 ns, selection of active channels), providing a live-view of incoming counter values and a live-chart depicting last 30 counter values. The gui is written in cpp using the qt-framework. The communication with the FPGA is done via a customized parallel protocol. For easy replication the authors can offer an image of the operating system.

A note on timing-characteristics:

In contrast to other approaches this setup is based on a synchronous pulse shortener using a phase-locked loop (pll) to multiply the driving system clock by a factor of eight instead of an asynchronous design. This leads to a reproducible behavior of the unit but led to a principle 5 ns-limit of the coincidence window width on this FPGA. Due to signal processing and FPGA internal behavior the system reaches in fact 6.6 ns, measured with an uncorrelated light source. This still meets the design-goal.